JOURNAL OF MATERIALS SCIENCE **40** (2005) 1993–2001

In-situ SEM observation on fracture behaviors of Sn-based solder alloys

DING YING, WANG CHUNQING
State Key Laboratory of Advanced Welding Production Technology, Harbin Institute of Technology, 92, Xidazhi Street, Nangang, Harbin 150001, People's Republic of China
E-mail: dyzoe@hit.edu.cn
E-mail: wangcq@hit.edu.cn

LI MINGYU
Shenzhen Graduate School of Harbin Institute of Technology, Xili Shenzhen University Town, Shenzhen 518055, People's Republic of China

BANG HAN-SUR
State Key Laboratory of Advanced Welding Production Technology, Harbin Institute of Technology, 92, Xidazhi Street, Nangang, Harbin 150001, People's Republic of China; Department of Naval Architecture and Ocean Engineering, Chosun University, 375, Seosek Dong, Donggu, Guangju 501-759, Korea

The effects of displacement rate on fracture behaviors of 100Sn solder and 63Sn37Pb solder alloys have been investigated by SEM *in-situ* testing. It was found that for the 100Sn solder, grain boundary sliding was the dominant deformation mechanism at lower tensile rate regime, while a large area of slip lines crossing grains were detected at the surface of specimens at higher tensile rate regime. For the 63Sn37Pb eutectic alloy, however, because of existence of the second phase, fracture behavior depended on the growth and linkage of cavities ahead of crack tip, and the crack paths changed from intergranular to transgranular with the increasing of loading rate.

1. Introduction

Solder joint reliability, the first issue in electronic interconnections, has received increasing attention in the last few decades, and considerable effort has been expended on both solder joints and bulk materials [1–3]. Much of the work has focused on isothermal fatigue, and several solder joint fatigue models have been proposed, such as Coffin-Manson, Solomon, Knecht, Fox and Akay etc. fatigue models [4]. However, the assumptions and applicability of these models vary, and there is no recognized universal conclusion made out. Lee *et al*. [4] demonstrated the primary limitation in fatigue modeling is all of these models do not adequately capture microstructural effects involving deformations and cracks. Pan [5] indicated that to model the solder deformation with cracking is a difficult task. Not only are modeling techniques involving propagating cracks still immature, but also the fracture characteristic of the bulk solder have not been well characterized as yet. In order to study solder joint reliability and predict its fatigue lifetime more successfully, the damage mechanism of solder alloys need to be researched more thoroughly.

Sn-based solder alloys have been widely used for electrical joints because of their low melting points, good wettability on copper, good plasticity, and reasonable electrical conductivity [6]. Due to their low melting temperature, the room temperature corresponds to a high homologous temperature ($T/T_m > 0.5$). In high homologous condition, time-dependent mechanisms, e.g., grain boundary sliding (GBS), cavitation and phase transformation, are possible to occur. These damage processes lead to premature failure of the solder. A lot of work has been done on failure mode and fracture mechanism of Sn-based alloys. Lee and Stone [7] found that GBS took place at strain rates below 10^{-3} s^{-1}($\sigma < 40$ MPa) and caused the initiation of intergranular cracks on the free surface of 63Sn-37Pb tensile-test specimens. For fatigue test, Kanchanomai *et al*. [8–10] found that wedge cracking due to GBS was the dominant mechanism of as-casted Sn-Pb eutectic solder when the strain rate was below 10^{-3} s^{-1}, while extensive cavitation was observed on the colony boundaries at higher strain rate than the value. Zhao *et al*. [11, 12] conducted fatigue crack growth tests of 95Pb-5Sn solder at frequencies from 0.01 to 10 Hz. They indicated that the fracture manner was changing from transgranular to intergranular with decreasing frequency. Fatigue crack growth under the frequency of 0.01 Hz was predominantly intergranular and time-dependent, while that under frequencies of 1 and 0.1 Hz was of mixed type but still cycle-dependent.

However, a limited amount of work has been done to study the dynamic development of cracks in Sn-based

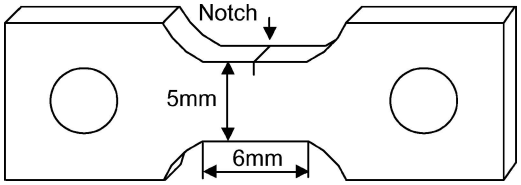

Figure 1 Specimen geometry and size.

alloys, and this is very important to understand the crack initiation and propagation in solder alloys. In this paper, the effects of loading rate on failure mechanism of 100Sn and 63Sn37Pb solder alloys were investigated. A transition from grain boundary behavior to intragranular dislocation strain was found, and the possible influencing causes were discussed in detail.

2. Material and experimental procedures

The materials used were pure tin solder, which was purified to 99.95% by distillation process, and 63Sn37Pb solder, which was as-cast and naturally aged at room temperature for at least one month to reach an equilibrium microstructure. Fig. 1 illustrates the specimen geometry and size. The thickness of the specimen was about 2.5 mm. For observation convenience, a notch was made in the middle of the specimen side face with linear cutting machine, as shown in the figure, and its depth was about 1 mm. The surface of the specimen was metallographically polished. Fig. 2 shows the optical and scanning electron microscope (SEM) images of the microstructures of 100Sn and 63Sn37Pb specimens respectively. It can be seen that the grain size of pure Sn is relative large, and the Sn-Pb eutectic alloy was consisted of Pb-rich phase (in the form of particles or needles, white) and β-Sn matrix (gray).

In-situ tensile experiment was conducted in a HITACHI S-570 SEM with a maximum load capacity of 2 kN at room temperature. Two kinds of displacement rate ($\dot{L}$) were employed, 0.05 and 1 mm min^{-1}. If using the strain rate as a standard, that equal to about below 10^{-3} s^{-1} and higher than the value. During *in-situ* tensile test, the straining was stopped several times in order to make the observations and take micrographs while the load was still applied.

3. Experimental results

3.1. Fracture behavior and mechanisms in the low loading rate regime ($\dot{L} = 0.05$ mm min^{-1})

3.1.1. 100Sn solder alloy

Fig. 3 shows the surface morphology of the 100Sn specimen during tensile process at low displacement rate. The loading direction was horizontal. It was found that the notch has been widened obviously. A lot of grain boundaries began to appear, that means intergranular slip was the dominant mechanism at early deformation stage, although slip lines were seen in some special locations, such as the zone near the notch where the plastic strain was concentrated.

On further loading, flow localization occurred and the area near the notch became a neck with centralized deformation. The surface presented uneven owing to grain rotation. This rotation was possibly resulted from non-equilibrium distribution of intergranular shear stresses, which means the pile-up dislocation along the grain boundary will supply the necessary torque that rotated the grain. With the straining increase, grains (like grain 'A') were elongated in the direction of tensile axis, and slip lines appeared within more grains.

A 'σ' shape void appeared at grain boundary ledge (the intersection between slip band and grain boundary, indicated by arrow) near the triple-point of grains during deformation process, as shown in Fig. 4. There might be two causes for the phenomena. On one hand, GBS would undoubtedly cause stress concentration at the interface between grains, which have different crystallography orientations. Moreover, the grain boundary was not smooth at all, a particle, even with an atom size, should become the obstacle of GBS. Generally assuming, if the stress concentration resulted from GBS cannot be eliminated quickly, the cavity might be nucleated along the grain boundaries. On the other hand [13], in the later stage of tensile, intragranular deformation was relative drastic, this nucleation of the void might be controlled by the build-up of internal stresses (local dislocation concentration) around grain boundary ledges as a result of incomplete plastic relaxation. Particularly, the grain boundary cavitation appears more readily under the condition of grain boundary sliding.

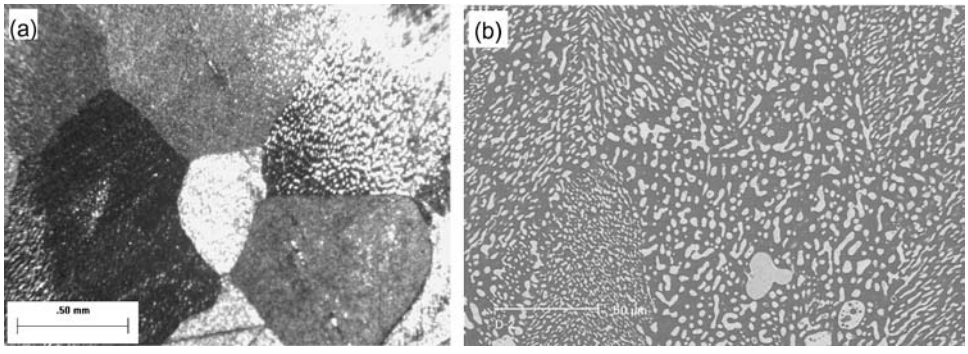

Figure 2 Microstructure of (a) 100Sn optical image and (b) 63Sn37Pb SEM image.

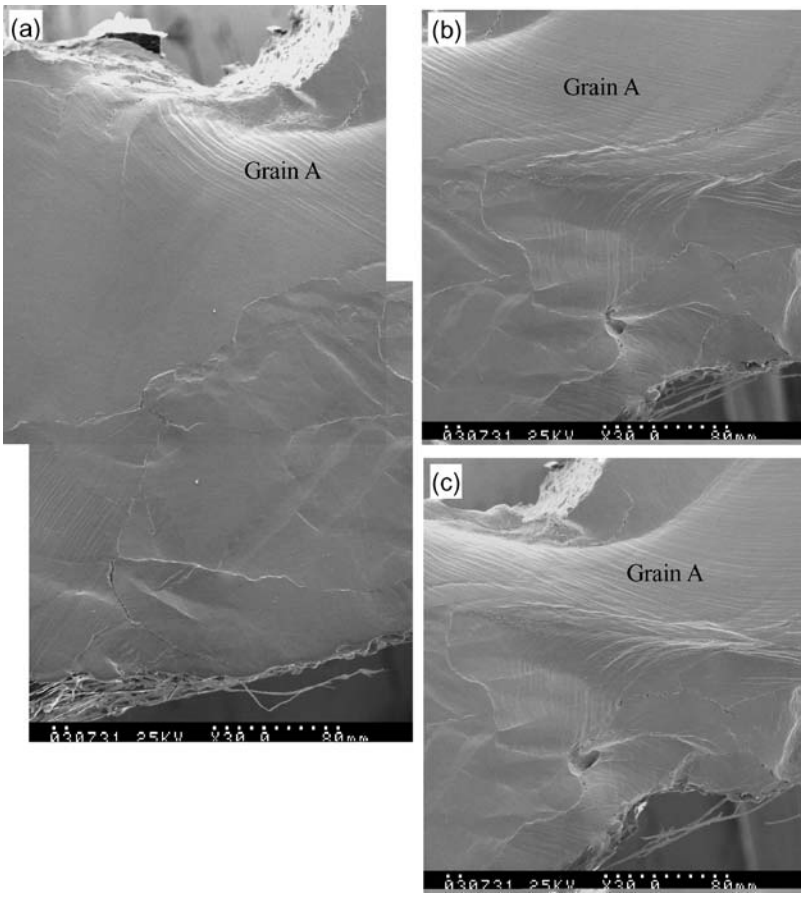

Figure 3 Macro deformation process of 100Sn specimen strained to (a) 5.7%, (b) 11.3% and (c) 17.8% at 298 K (low displacement rate, $\dot{L} = 0.05$ mm min^{-1}, load direction in horizontal).

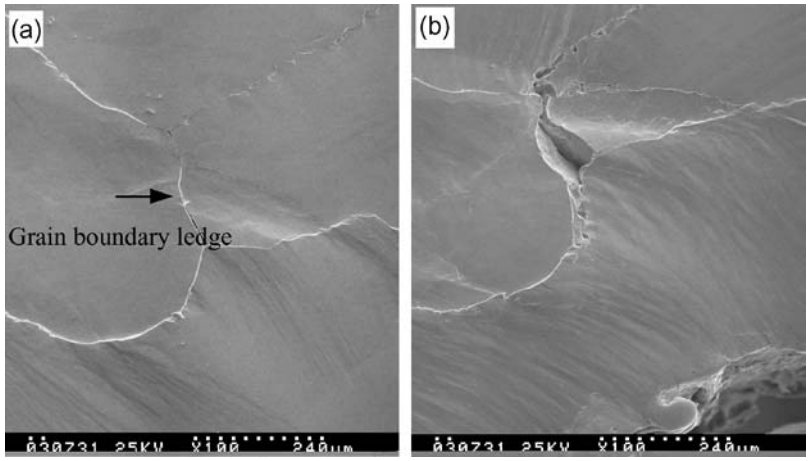

Figure 4 Damage information near the triple-point of grain junctions in 100Sn specimen strained to (a) 2.1% and (b) 5.7% at 298 K (low displacement rate, $\dot{L} = 0.05$ mm min^{-1}, load direction in horizontal).

Local distortion behavior could further demonstrate the deformation mechanism of 100Sn specimen at low displacement rate. A scratch crossing two grains made on the specimen surface before test was staggered a little, which indicated the occurrence of GBS (see Fig. 5). Simultaneously, dislocation glide was acted inside the grain also, as shown in Fig. 6. Above all, it can be conferred that grain boundary sliding was the dominant mechanism of 100Sn specimen in the case of this loading rate, accompanied by some intragranular slips, which became more remarkable after the narrow neck was formed.

3.1.2. 63Sn37Pb solder alloy

With joining the second phase, lead, fracture behavior was different from the pure tin. Fig. 7 shows a sequence of crack propagation near the notch at the early stage of loading. The crack was initiated from the intersection of notch side face and grain boundary due to stress concentration. Meanwhile, a triple-point of grain junction inside the specimen, as indicated by arrow in Fig. 7, became the position where a cavity nucleated and grew up gradually. The crack near the notch attempted to meet the cavity, but impeded by the grain 'B'. Finally, grain 'B' was drawn apart singly from the structure, rather

Figure 5 Staggered lines crossing grain boundaries showed the occurrence of GBS in 100Sn solder (2.1% strain at 298 K, low displacement rate, $\dot{L} = 0.05$ mm min^{-1}, load direction in horizontal).

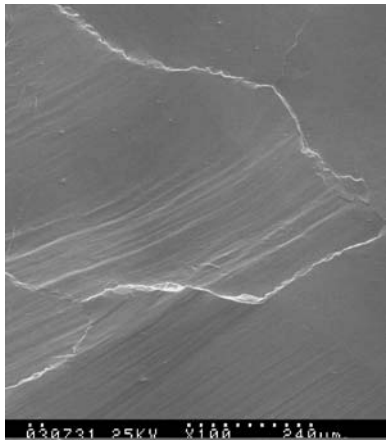

Figure 6 Slip lines within the grain of 100Sn solder strained to 2.9% at 298 K (low displacement rate, $\dot{L} = 0.05$ mm min^{-1}, load direction in horizontal).

than traversed. This process proved the intergranular cracking mechanism for 63Sn37Pb specimen at this loading rate.

The specific evolution of point 'C' was shown in Fig. 8. It can be seen that the triple-point of grain junction where the boundary sliding might be blocked is the preferential position for cavity nucleation. The second phase particles on boundary could not deform harmoniously with matrix when grain boundary slides, especially to the large particle that has weaker combination with the matrix. Cavities are easy to form here, as indicated in Fig. 8a. At the same time, straining in the area between the cavity and the crack tip was increased drastically owing to their growth. This resulted in the pulling off or fracture of many small particles, as shown in Fig. 8c, there a lot of fine Pb rich particles were separated from Sn matrix.

Since the growth of initial crack was limited in the depth direction owing to the obstacle (grain 'B'), a new crack on the right side of notch was generated and propagated sharply at later stage of tensile process (see Fig. 9a). It should be noted that the directions of grain boundary sliding are normally in the maximum shear stress direction, this made the major crack propagate in 45° angle to the loading direction. With high magnification of crack tip in Fig. 9b, it can be known that as the interphase boundaries can be considered as weak areas with high free-energy, sliding process, stress concentration, diffusion process and consequently cavities can be easily nucleated in these areas. Because of straining concentration, the stripe-like Pb rich phase on the right of crack tip and particle-shape Pb rich phase on the left were all separated from matrix. Cavities can be observed along the crack tip one after another, as indicated in Fig. 9b, they accelerated the crack propagation and resulted in the final failure.

Thus, although the second phase particles that hold back the movement of dislocations effectively, behave as strengthening part that enhances the strength of the solder. However, just because of their existence also, the boundary sliding will rise up the stress concentration at these irregularities along the boundaries. This high stress magnitude can locally damage the boundaries and induce some cavities.

For the displacement rate of 0.05 mm min^{-1}, the deformation of pure tin depended on boundary sliding, grain rotation, accompanied with intragranular slip partially, so that the stress concentration was relaxed. During this process, grain boundaries were migrated continuously, until the grains were elongated notably and the neck was formed that resulted in the final failure. After adding the lead in solder, however, boundary sliding was reduced when fine particles of second phase were present in the grain boundary. This result stabled boundaries to some extent. Therefore, around triple-point grain corner area or along grain (interphase) boundaries, cavities nucleated by impurities or second phase particles can be observed due to stress concentration. On further loading, the failure was characterized by intergranular cracking due to formation of cavities along the grain boundaries and then linkage and propagation.

3.2. Fracture behavior and mechanisms in the high loading rate regime ($\dot{L} = 1$ mm min^{-1})

3.2.1. 100Sn solder alloy

Fig. 10 shows the macro deformation process of 100Sn specimen at high displacement rate. A great deal of slip lines was observed at the area near the notch, which provides the evidence of heavy intragranular deformation. As for the area far away from the notch, since the straining there was relative small at early tensile stage, only a small amount of dislocations near the boundaries need to be activated to relax the stress concentration. Corresponding boundary behavior made a few grains emerged, as shown in Fig. 10a. While on further straining, stress intensity increased quickly at such a high rate, and the contribution from GBS is not expected to relax so much stress concentration, which resulted in that intraganular deformation would assume greater significance then. Finally, large grains with slip bands were ripped and transgranular fracture occurred.

Deformation mechanism of 100Sn specimen at high tensile rate can be demonstrated more evidently for the observation of local deformation phenomena. The high

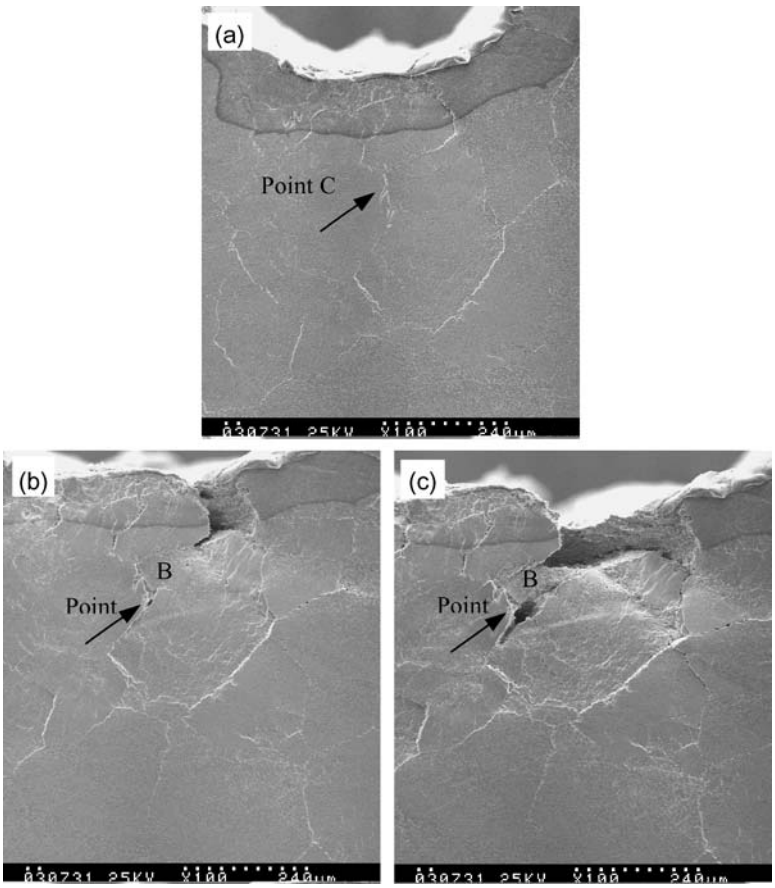

Figure 7 A sequence of crack propagation near the notch of 63Sn37Pb specimen strained to (a) 1.7%, (b) 2.9% and (c) 4.6% at 298 K in early tensile stage (low displacement rate, $\dot{L} = 0.05$ mm min^{-1}, load direction in horizontal).

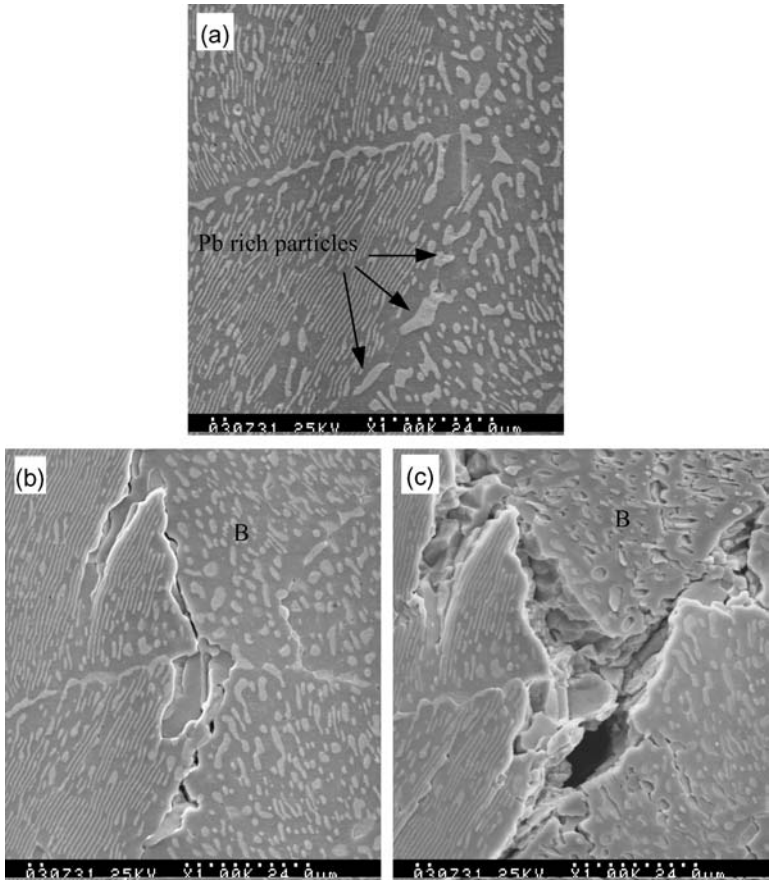

Figure 8 Damage evolution near the triple-grain junctions in 63Sn37Pb specimen during tensile process strained to (a) 0%, (b) 1.7% and (c) 2.9% at 298 K (low displacement rate, $\dot{L} = 0.05$ mm min^{-1}, load direction in horizontal).

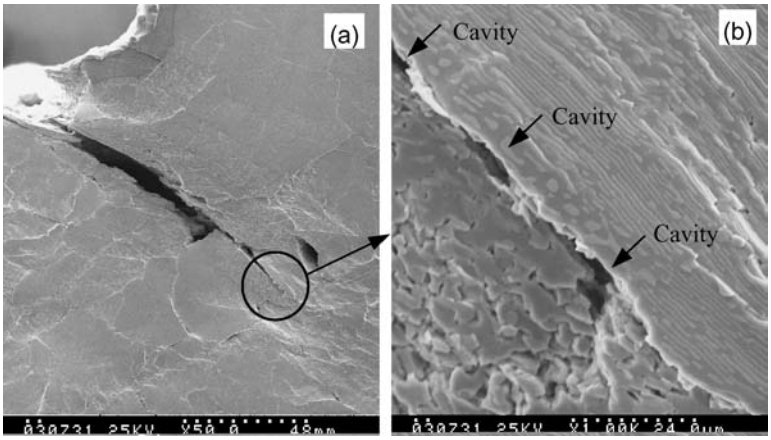

Figure 9 Main crack propagation of 63Sn37Pb solder specimen strained to 18.1% at 298 K with (a) low magnification and (b) high magnification of crack tip (low displacement rate, $\dot{L} = 0.05$ mm min^{-1}, load direction in horizontal).

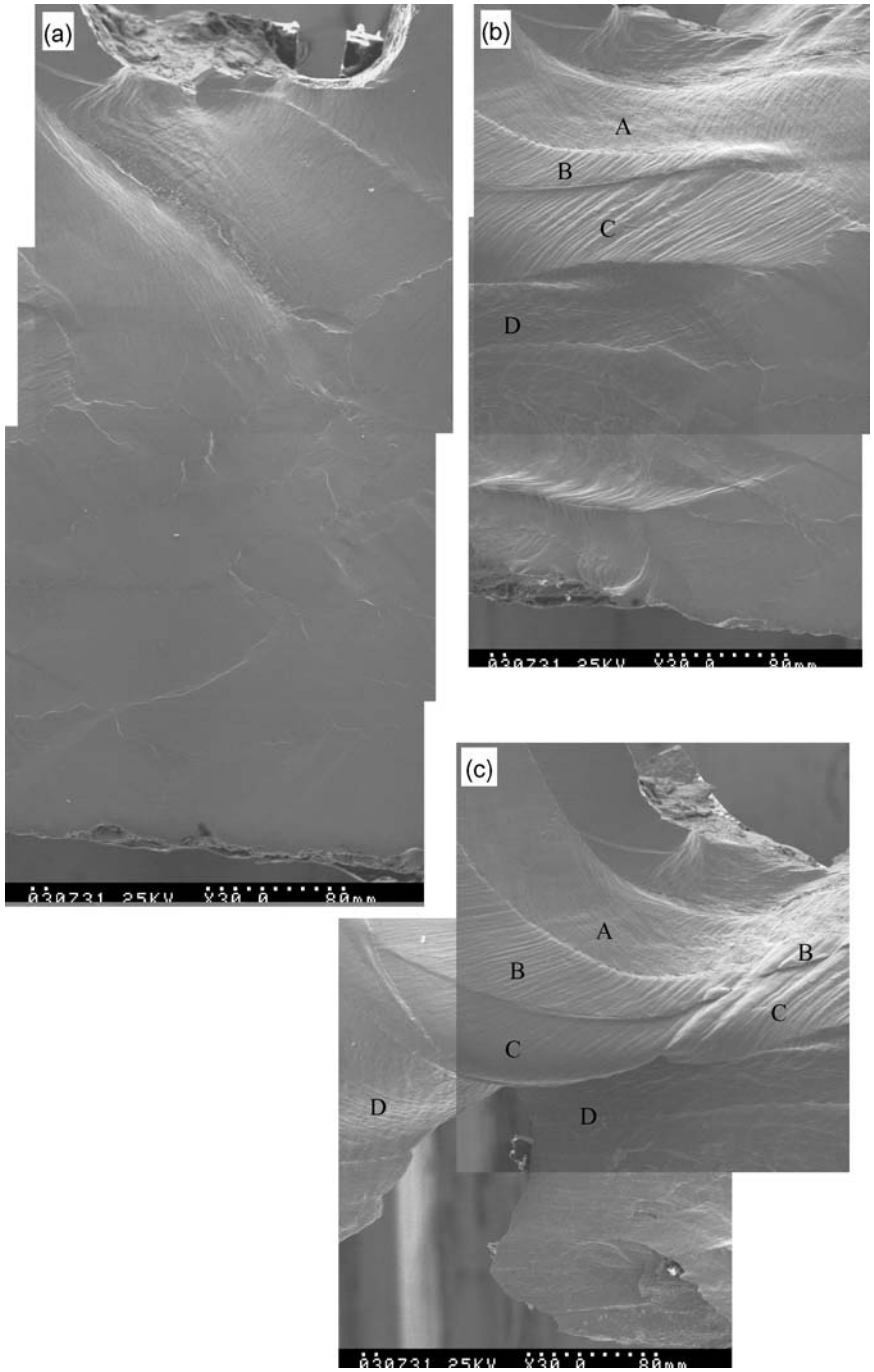

Figure 10 Marco deformation process of 100Sn specimen strained to (a) 3.9%, (b) 7.8% and (c) 9.1% at 298 K (high displacement rate, $\dot{L} = 1$ mm min^{-1}, load direction in horizontal).

Figure 11 Secondary slip lines near the notch of 100Sn specimen strained to 7.8% at 298 K (high displacement rate, $\dot{L} = 1$ mm min^{-1}, load direction in horizontal).

flow stress in the place under the notch got the critical shear stress that activated the second slip system, and cross sliding caused the dislocation web, as shown in Fig. 11. After the increase of intragranular dislocation slide, a large amount of slide behavior could satisfy the deformation of many grains, this decreased the stress gratitude along grain boundaries, and consequently boundary behavior was limited further. See Fig. 12, the defect position on the grain boundary differed little during tensile process. So for high loading rate tests, the deformation of grain matrix without GBS controlled flow behavior. It should be noted that although both specimen surfaces tested at high and low tensile rates showed GBS and grain matrix deformation, GBS was more dominant at lower rate and intragranular deformation was more remarkable at higher rate.

3.2.2. 63Sn37Pb solder alloy

For 63Sn37Pb specimens tested at higher tensile rate, fracture was predominantly transgranular, along with the linkage of the voids ahead of crack tip, as can be seen from Fig. 13. Therefore, no matter for intergranular fracture at low displacement rate or transgranular failure at high displacement rate, link up of the cavities to form major cracks were always involved in Sn-Pb eutectic alloy.

It should be concluded the elevation of tensile rate regime made the fracture mechanism of Sn-based solder alloys changed from intergranular to transgranular. Here, we can borrow some ideas in super-plastic

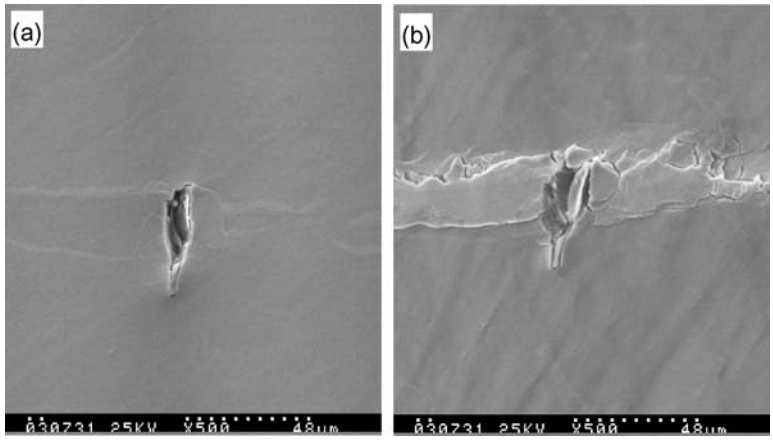

Figure 12 Variation of defect on the grain boundary of 100Sn specimen strained to (a) 2.4% and (b) 11.7% at 298 K (high displacement rate, $\dot{L} = 1$ mm min^{-1}, load direction in horizontal).

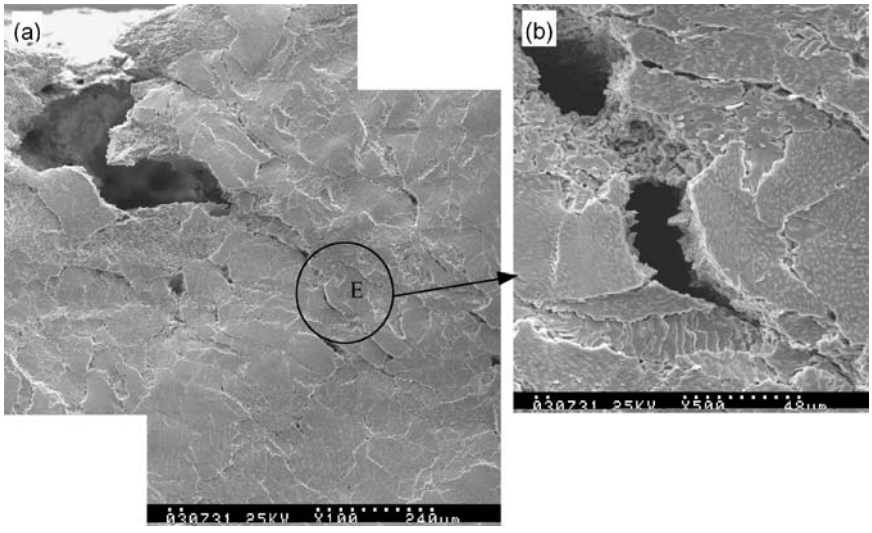

Figure 13 Main crack propagation of 63Sn37Pb solder specimen strained to 5.1% at 298 K with (a) low magnification and (b) high magnification of crack tip (high displacement rate, $\dot{L} = 1$ mm min^{-1}, load direction in horizontal).

realm. Gifkins presented "Core-Mantle" theory [14], and he indicated that dislocations were concentrated at a very thin zone closing to grain boundary, without dislocations near the core. When deformation was carried out at a proper and lower tensile rate, boundary sliding just occurred within a very narrow and viscous mantle surrounding the rigid grain core. With the increasing of tensile rate, however, the mantle was increased in depth also, until dislocations were distributed in the whole grain at very high loading rate. That means boundary sliding could not keep up with the tensile rate, resulted in dislocation accumulation on microstructure of alloys. Consequently deformation was transferred from one grain to the other, by this means the material was distorted, that is the common property of general plastic deformation.

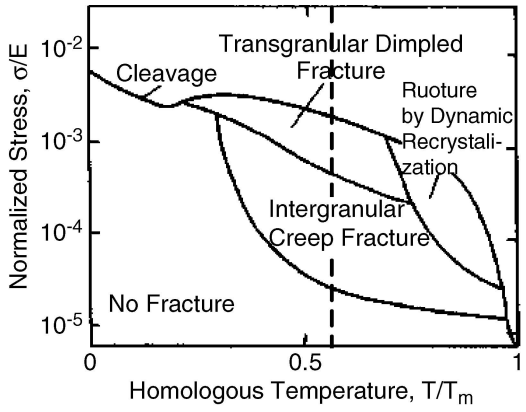

Figure 14 Schematic illustration of Fracture mechanism.

4. Discussion

4.1. Effect of Sn crystal structure

The deformation property of Sn-based solder could be traced to crystal structure of pure tin (β-Sn) that belongs to pyramidal system. The lattice parameters are expressed as $a = b = 0.58197$ nm, $c = 0.31750$ nm, and the radius of atom is 0.158 nm. Its enthalpy of vacancy forming energy is only 0.5 eV, that means vacancies are easily to form in the metal. Furthermore, notable anisotropic property of this crystal structure made the difference between hard and soft orientation large. While normally in polycrystal, the grains must maintain their continuity, so that the boundaries between the deforming grains remain intact. However each grain tries to deform in its best orientation, the constraints imposed by continuity cause differences in the deformation between neighboring grains. Consequently the intense stress concentration along boundaries can be speculated. Together with high homologous temperature condition, the atom mobility and vacancy diffusion capacity were relatively high, and the grain boundaries, which have high surface energy, naturally served as preferential locations for solid-state process, just like diffusion. In this situation, the boundaries become slippery and weaker than the matrix. Therefore the boundary sliding, which is one of the primary sources of high-temperature fracture mechanism, is able to occur for Sn-based solder alloys studied here.

4.2. Effect of loading condition

The relationships in simplified form between the normalized stress and homologous temperature are shown in Fig. 14 [15]. At ambient temperature, the value of T/T_m for 100Sn is about 0.59, and the value of T/T_m for 63Sn37Pb is about 0.65, as indicated by the dashed line in the figure. It can be conferred that at this homologous temperature, plastic flow is easily to proceed when the normalized stress was elevated quickly. For the Sn-Pb eutectic solder, voids will continuously grow as long as the load stress was below the instant rupture stress, and fracture occurred after a certain of hold time. For the pure tin, because of the absence of particles nucleated for voids, grains were teared up finally by plastic flow and resulted in the failure.

While at lower normalized stress level and experiencing longer time, namely the deformation rate is relative low, atoms or vacancies have enough time to move to the boundary, and high temperature diffusion mechanism is activated fully. At this stress-temperature regime, the diffusion of atom or vacancy in the stress direction provides the condition for voids growing up, and materials deform owing to creep controlled by dislocation climb. For the pure tin, continuous boundary sliding and boundary transference resulted in the growth of grains and final destabilization and failure. For the Sn-Pb eutectic alloy, fracture depended on link up of cavities along boundaries. With regard to the mechanism of cavitation on grain boundary at elevated temperature, there are two main theoretical explanations. One is an extension of the low-temperature mechanism for the nucleation of voids at grain boundary ledges, or second phase particles, which was mentioned in previous statement on Fig. 4. This nucleation is controlled by the build-up of internal stresses (local dislocation concentration) around grain boundary ledges or particles as a result of incomplete plastic relaxation. The second mechanism invokes the clustering of vacancies to form (by diffusion) a void cluster [16]. The model describing this mechanism predicts that (a) cavities are most probably formed at second-phase particles on the grain boundary; (b) they can be formed even when the normal stress at the particle–matrix interface is smaller than the theoretical fracture strength of the interface; (c) the probability of cavity nucleation is the highest at the perimeter of contact between the particle and the grain boundary; and (d) in addition to a threshold stress, an incubation time must elapse before enough vacancies can cluster together (by diffusion) to form a void of critical size. In the present study, to the voids observed in Sn-Pb eutectic solder, as shown in Fig. 8, the second viewpoint for the nucleation of void seems to be operative.

4.3. Explanation of traditional dislocation theory

The peak loads of both specimens at two displacement rates during tensile process were shown in Fig. 15. It might be explained by Taylor yielding strength

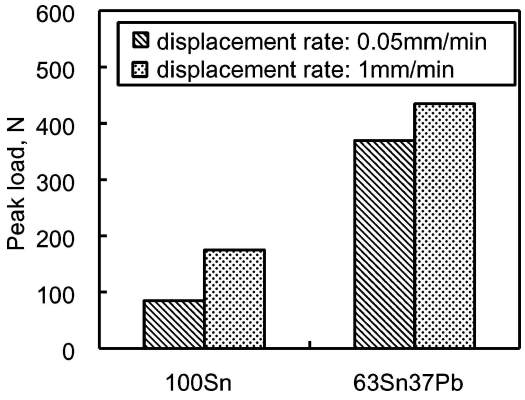

Figure 15 Peak loads of both specimens at two displacement rates during tensile process.

expression based on dislocation theory [15]:

$$\tau_y = \alpha G b \sqrt{\rho}, \tag{1}$$

where, b is burgers vector modulus, ρ is dislocation density, α is geometric constant, and G is shear modulus. So yielding strength of plastic material has relations with inside dislocation density. Combing formulation (1) with the information from Fig. 15, it can be known at low tensile rate, dislocation behavior was centralized along grain boundaries, deformation mechanism was dislocation sliding accompanied by dislocation climb that belongs to a kind of dynamic recovery process, namely dislocation creep. Dislocation density then was relative small, the peak load was also small, and the failure of specimen was intergranular. Under high tensile rate, however, grain boundary behavior could not keep up with the tensile rate, a great deal of dislocations were distributed within grains, and consequently work-hardening phenomena was great. Thus the maximal bearing load was higher. Similarly, joining of second phase blocked the dislocation movement. As a result, dislocation density was increased that caused the strength of Sn-Pb eutectic solder higher than pure tin.

Furthermore, plastic deformation rate is also proportional to the instant dislocation density. The following is the famous Orowan formulation:

$$\dot{\varepsilon} = \Phi b \rho_{\text{mob}} v_{\text{mob}} \tag{2}$$

where ρ_{mob} is density of mobile dislocations, v_{mob} is average velocity of mobile dislocations, and Φ is geometric factor, the Schmid factor for single crystal or the reciprocal of Taylor factor for polycrystal, which has relationship with resolving shear stress τ, resolving strain increment $\mathrm{d}\gamma$, tensile stress tensile σ, and strain increment $\mathrm{d}\varepsilon$, expressed as:

$$\Phi = \frac{\tau}{\sigma} = \frac{\mathrm{d}\varepsilon}{\mathrm{d}\gamma} \tag{3}$$

Therefore, dislocation accumulation could be more significant under high loading rate compared to low rate tests and this probably is another reason for intragranular deformation at high rate, but intergranular behavior at low rate.

5. Conclusion

The effect of displacement rate on fracture behaviors of 100Sn and Sn63Pb37 solder alloys have been studied by *in-situ* SEM tensile testing method at ambient temperature. The main conclusions obtained are summarized as follows: For the pure tin, grain boundary sliding was dominant mechanism in the low tensile rate regime, boundaries continuously transferred and grains were elongated in loading direction. While intragranular deformation was dominant mechanism in high tensile rate regime, a great deal of slip bands appeared, and the specimen was ripped transgranularly. For the Sn-Pb eutectic solder, cavities were nucleated along grain boundaries owing to the presence of second phase particles. Crack propagation depended on the link up of these cavities, and failure mode was intergranular at low tensile rate regime. With the loading rate increasing, however, fracture occurred in transgranular form by connecting the voids ahead of crack tip.

Acknowledgement

The authors gratefully acknowledge Institute of Mechanics, Chinese academy of sciences for the support during testing process.

References

1. S. VAYNMAN, G. GHOSH and M. E. FINE, *J. Electron. Mater.* **27**(11) (1998) 1223.
2. M. E. FINE, V. STOLKARTS and L. M. KEER, *Mater. Sci. Eng.* A **272** (1999) 5.
3. S. RUSSELL, A. GRIGALS and E. CLEMENTE, *J. Electron. Mater.* **28**(9) (1999) 1008.
4. W. W. LEE, L. T. NGUYEN and G. S. SELVADURAY, *Microelectr. Relia.* **40** (2000) 231.
5. TSUNG-YU PAN, *IEEE Trans. CHMT* **14**(4) 824.
6. S. K. KANG and A. K. SARKHEL, *J. Electron. Mater.* **23**(8) (1994) 701.
7. S. M. LEE and D. S. STONE, *Scripta Metallur. et Mater.* **30**(9) (1994) 1213.
8. C. KANCHANOMAI, Y. MIYASHITA and Y. MUTOCH, *Int. J. Fatigue* **24** (2002) 987.
9. C. KANCHANOMAI, S. YAMAMOTO, Y. MIYASHITA, Y. MUTOH and A. J. MC EVILY, *ibid.* **24** (2002) 57.
10. C. KANCHANOMAI, Y. MIYASHITA and Y. MUTOH, *ibid.* **24** (2002) 671.
11. J. ZHAO, Y. MIYASHITA and Y. MUTOH, *ibid* **22** (2000) 665.
12. *Idem.*, *ibid.* **23** (2001) 723.
13. S. H. GOOD and L. M. BROWN, *Acta Metallur.* **27** (1979) 1.
14. R. C. GIFKINS, *Scripta Metallur. et Mater.* **25**(6) (1991) 1397.
15. HAEL MUGHRABI-WEINHEIM, in "Materials Science and Technology: A Comprehensive Treatment" (Cambridge, New York, 1998) p. 7.
16. R. RAI and M. F. ASHBY, *Acta Metallur.* **23** (1975) 653.

Received 3 March
and accepted 20 July 2004